"OBSERVATIONS OF PRECIPITABLE WATER VAPOR ALONG THE MARITIME CONTINENT ASSOCIATED WITH EL NIÑO-SOUTHERN OSCILLATION ACTIVITY"

Wayan Suparta[1,*]

[1] Department of Doctor of Computer Science, Bina Nusantara University, Jakarta, Indonesia

ABSTRACT

The effect of El Niño and La Niña events is a major issue in the regional climate of Southeast Asia. This study uses the Precipitable Water Vapor (PWV) values estimated from Global Navigation Satellite System (GNSS; in particular Global Positioning System, GPS) to investigate the El Niño-Southern Oscillation (ENSO) activity in the Southern coast of the South China Sea (SCS). For this study, GPS and meteorological systems are installed at the Universiti Malaysia Sabah, Kota Kinabalu (UMSK), which is located on the coast of the maritime continent. Subsequently, PWV from GPS and PWV obtained from Radiosonde, prior to the investigation of ENSO activity, are compared. To further investigate the relationship between PWV and ENSO activities, data from three additional GPS stations located along the coast of SCS during the 3-year period 2009-2011 were analyzed. The selection period considers the availability of GPS data. The obtained results show that during the increased intensity of El Niño in 2009/2010, PWV decreases and drops about 10-week later, i.e., after the sea surface temperature anomaly (SSTa) has peaked. PWV has a negative correlation with the El Niño index, which is comparable with precipitation data obtained from NASA's Tropical Rainfall Measuring Mission (TRMM). In contrast, the amount of PWV was increased during the La Niña event of 2010/2011. This observation suggests the GPS is a suitable technique for studying the ENSO activity.

1. INTRODUCTION

Seasonal El Niño-Southern Oscillation (ENSO) episodes coupled with the warming of central and the eastern Pacific Ocean lead directly to substantial shifts in weather patterns across the Pacific. Origination of ENSO activities in the tropical Pacific affected the human life and the environment throughout weather events, such as drought/flooding, landslides, and tropical storms. Pokhrel et al. [2012] summarize this phenomenon by considering monsoon circulation, which indicates that ENSO occurs inter-annually, on a periodic timescale of 2 - 7 years, and can even affect its seasonal pattern [Chen and Lin, 2005]. However, several aspects of ENSO that may affect particular regions are still not entirely understood. ENSO is a complex ocean-atmosphere coupling phenomenon that is followed by extreme, and sometimes unusual, weather patterns at distinct locations around the globe. The effects of ENSO phenomenon are widespread throughout the hemisphere, including Southeast Asia, and remain periodically active near Borneo region from December to January [Qian et al., 2013]. Therefore, monitoring and forecasting of ENSO cycles and their modes are important to take into account their impact on the global climate.

Water vapor is a key atmospheric component and has an extremely important role in weather patterns. It is an important factor in inducing climate change and contributes to the positive feedback loop that amplifies externally forced climate fluctuations [Bajželj and

Richards, 2014]. Investigation of water vapor variability associated with ENSO is important to better understand the global climate system. For that purpose, the Global Positioning System (GPS) has been extensively used as an effective tool to measure atmospheric water vapor in all weather conditions and on a global scale. Monitoring the water vapor from GPS, and in particular the so-called as the precipitable water vapor (PWV), was proposed for the first time by Bevis et al. [1992]. Fluctuation of PWV can be detected from the wet delay of GPS signals in the neutral atmosphere due to inhomogeneous atmospheric density. This method is a form of low-cost technology and has proven to be useful in detecting climate change.

Up to date, only a few studies have dealt with ENSO activities by using GPS data. Suparta et al. [2013] reported the observation of GPS PWV variability over the western Pacific Oceans during a La Niña event in Niño 4 regions. The analysis used one-year data (acquired on 2011) and found that the amount of PWV was increased due to strong trade winds and mass of the warm water moving from central to the west Pacific. The present study investigates the correlation between PWV and ENSO activity along the South China Sea (SCS). The advantage of exploiting PWV products from GPS with respect to that obtained from Radiosonde measurements is also discussed, thus confirming that GPS observations is a suitable technique to study water vapor dynamics during ENSO events. In addition, the relationship between PWV and ENSO episodes is discussed using the precipitation data obtained from NASA's Tropical Rainfall Measuring Mission (TRMM).

2. METHODOLOGY

2.1 DATA AND LOCATION

SCS is an important link between the western Pacific Ocean and the Indian Ocean, and the climate systems. This interaction plays an important role in regulating the climate over the Maritime Continent and nearby regions, including Borneo and Philippines. From the four Niño regions (1+2, 3, 3.4, and 4), Niño 3.4 anomalies had the higher impact in the ocean-atmosphere interactions across the Pacific region as compared to other Niño regions [Trenberth, 1997]. Therefore, 3-year of data, from 1 January 2009 to 31 December 2011 (Modified Julian Date (MJD): 54832 - 55926), in four selected locations along SCS, which cover episodes of both El Niño and La Niña events, were collected and analyzed. Since GPS system at UMSK just started to operate at the end of March 2011, another GPS data set used for com-

parison was obtained from Manila Observatory (PIMO) in the Philippines and Nanyang Technological University of Singapore (NTUS) in Singapore. GPS data for PIMO and NTUS were downloaded from the Scripps Orbit and Permanent Array Center (SOPAC) website (http://sopac.ucsd.edu/).

GPS PWV results were then compared with PWV data taken from Radiosonde measurements (RS PWV). RS PWV data were provided by Wyoming University (http://weather.uwyo.edu/upperair/sounding.html). In this work, GPS data obtained at UMSK were compared with RS data obtained at WBKK (96471: Kota Kinabalu Airport) in Borneo region, while GPS data obtained at PIMO were compared with RS data obtained at TANAY (98433: Calabarzon, Philippines). Note that the value in the bracket of each station is the ID code assigned by the World Meteorological Organization (WMO). Figure 1 shows the location of GPS stations together with three RS stations. The figure also shows the location the RS stations VVTS (48900: Tân Sơn Nhất International Airport) at Ho Chi Minh city, Vietnam (Tân Sơn Nhất Airport) which is along the coast of SCS path. The geographical location of GPS and RS stations used in this study are summarized in Table 1.

To compare the climate response through PWV measurements during ENSO episodes, precipitation data from NASA's Tropical Rainfall Measuring Mission (TRMM) are collected. Daily 3B42 V7 products for the region: 100°E-125°E and 0°-16°N are retrieved by TRMM Online Visualization and Analysis System (TOVAS), while monthly data are denoted with the 3B43 code. Data can be obtained through NASA website (http://gdata1.sci.gsfc.nasa.gov/daac-bin/G3/gui.cgi?instance_id=TRMM_3B42_Daily). To indicate the occurrence of ENSO events, sea surface temperature anomaly (SSTa) data are also collected from NOAA website (http://www.cpc.ncep.noaa.gov/data/indices/sstoi.indices). Details on SSTa and its relation with El Niño and La Nina are described in the next section.

2.2 DATA PROCESSING

At UMSK, the GPS receiver records data every 30 seconds, whilst surface meteorological data (pressure P in mbar, temperature T in °C, and relative humidity RH in percent) are recorded at one-minute intervals. At this station, meteorological sensors (MET4A) are co-located with the GPS receivers. These instruments have accuracies of ±0.08 hPa, ±0.1°C and ±2% for P, T, and RH, respectively. Both GPS signals and surface meteorological data were processed to calculate PWV. When meteorological sensors are not co-located with a GPS receiver (for example, TANAY and PIMO), the P, T, and RH val-

Global Positioning System (GPS)				Radiosonde (RS)			
Station ID (Country)	Latitude (Deg.)	Longitude (Deg.)	Height (m)	Station ID (Country)	Latitude (Deg.)	Longitude (Deg.)	Height (m)
UMSK (Malaysia)	6.03 N	116.12 E	63.49	WBKK (Malaysia)	5.93 N	116.05 E	3.0
NTUS (Singapore)	1.35 N	103.68 E	75.38	VVTS (Vietnam)	10.81 N	106.66 E	10.0
PIMO (Philippines)	14.64 N	121.08 E	95.53	TANAY (Philippines)	14.56 N	121.36 E	45.6

TABLE 1. Geographical coordinates of the GPS and RS stations used in this study.

ues at the GPS position were interpolated using the method proposed by Klein Baltink et al. [1999]. Once the GPS and surface meteorological data have undergone such a pre-processing, the total value of Zenith Tropospheric Delay (ZTD) can be calculated, which is an intermediate step to finally compute PWV. In turn, ZTD is the sum of the Zenith Hydrostatic Delay (ZHD) and Zenith Wet Delay (ZWD). The ZTD is calculated based on the improved Modified Hopfield model [Hofmann-Wellenhof et al., 2001; Suparta et al., 2008] as a function of P, T, RH, θ, which can be expressed as

$$ZTD(P,T,RH,\theta)=10^{-6}N_{j,0}^{Trop}\left[\sum_{k=1}^{9}\frac{\alpha_{k,j}}{j}r_j^k\right] \quad (1)$$

where

$$\begin{aligned}
&\alpha_{1,j}=1 \\
&\alpha_{2,j}=4a_j \\
&\alpha_{3,j}=6a_j^2+4b_j \\
&\alpha_{4,j}=4a_j\left(a_j^2+3b_j\right) \\
&\alpha_{4,j}=a_j^4+12a_j^2b_j+6b_j^2
\end{aligned}
\qquad
\begin{aligned}
&\alpha_{6,j}=4a_jb_j\left(a_j^2+3b_j\right) \\
&\alpha_{7,j}=b_j^2\left(6a_j^2+4b_j\right) \\
&\alpha_{8,j}=4a_jb_j^3 \\
&\alpha_{9,j}=b_j^4
\end{aligned}
\quad (2)$$

and

$$a_j=-\frac{\sin\theta}{h_j} \text{ and } b_j=-\frac{\cos^2\theta}{2h_jR_E} \quad (3)$$

where $N_{j,0}^{Trop}$ is the refractivity at the surface of the earth, k is layer (1...9), α is a series expansion of tropospheric layer, and r_j is the dry and wet refractivity components as a function of tracking station height h above the Earth's surface. The length of r_j is measured from the center of the Earth, thus the value of the Earth radius (R_E = 6378137 meters) is taken into account, and $a = R_E \cos\theta$. The elevation angle (θ) is obtained from GPS reading. The solution to the r_j based on the expansion series is given as follows:

$$r_j=\left[R_E^2\left(1+\frac{h_j}{R_E}\right)^2-a^2\right]^{\frac{1}{2}}-\left[R_E^2-a^2\right]^{\frac{1}{2}} \quad (4)$$

Noted that for the hydrostatic refractivity component, the subscript j is replaced by hyd and for the wet refractivity component is replaced by wet, respectively. In Equation (4), h_j (in meters) stands for h_{hyd} and h_{wet} that are the effective heights for the hydrostatic and wet components, respectively. In this work, the input to calculate the ZTD is the elevation angle and surface meteorological data (P, T, and RH). A Vienna mapping function (VMF1) was used to reduce atmospheric bias in the ZTD estimation [Suparta et al., 2011].

On the other hand, the ZHD was calculated using the Saastamoinen model [Saastamoinen, 1972]. The input to obtain the ZHD value is surface pressure (P_s), latitude of the station (φ) and the height of the site above the ellipsoid (h, in km) as given by

$$ZHD=(0.0022768\pm0.0024)\frac{Ps}{f(\varphi,h)} \quad (5)$$

$$f(\varphi,h)=1-0.00266\cos(2\varphi)-0.00028h \quad (6)$$

where $f(\varphi,h)$ is a correction factor to correct for the local gravitational acceleration at the center of mass of the atmospheric column.

The ZWD was computed by subtracting the ZHD from ZTD ($ZWD=ZTD-ZHD$). ZWD was then transformed into an estimate of the PWV based on the surface temperature measured at a particular site. PWV total (in mm) from a receiver to the top of the atmosphere was calculated based on the formula proposed by Bevis et al. [1992].

$$PWV=\pi(T_m)\,ZWD, \text{ where } \pi(T_m)=\left[\rho_{lw}R_v\left(\frac{k_3}{T_m}+k_2'\right)\right]^{-1}10^6 \quad (7)$$

where the dimensionless $\pi(T_m)$ is a conversion factor that varies with local climates such as location, eleva-

tion, season and weather. ρ_{lw} and R_v are the density of the liquid water (1000 kg m^{-3}) and specific gas constant for water vapour (461.5184 J mol^{-1} K^{-1}), the refraction constants k_1 = (77.6 $\pm$ 0.05) K mbar^{-1}, k_2 = (22.1 $\pm$ 2.2) K mbar^{-1} and k_3 = (3.739 $\pm$ 0.012) x 10^5 K^2 mbar^{-1} are computed as in Bevis et al. (1994). Originally, the mean temperature T_m in Equation 6 is for middle regions and is estimated based on the Davis et al. [1985] formula. Since the location of this study is in the tropical region, Radiosonde data in 15 sites over the Western Pacific region were collected to estimate the new T_m formula as in Equation 8 [Suparta and Iskandar, 2013].

$$T_m = 0.83663 \ T_s + 48.103. \tag{8}$$

T_s is the local surface temperature measured at the site (in Kelvin). More details concerning the instrument and algorithm used in this work to determine PWV from ground-based GPS observations can be found in Suparta et al. [2008].

To process and analyze the above parameters, a tropospheric water vapor program (*TroWav*; a set of Matlab™ codes) developed by Suparta [2014] was employed. A correlation analysis based on the R-squared (R^2) values was applied to study the relationship between GPS PWV and ENSO activity. The R^2, or coefficient of determination, is the square of the Pearson's correlation coefficient (*r*) and represents the goodness of fit, or the usefulness of the statistical model analysis, to assess two measurement variables. Note that the relationship between the occurrence of ENSO and the PWV response is examined referring as for the ENSO occurrence to the SSTa Oceanic Niño Index (ONI) intensity, as defined by the Japan Meteorological Agency (JMA) [1991] in pathways of the Niño 3.4. The index is calculated as a 5-month moving average of spatially averaged SST anomalies over the tropical Pacific, in the region 5°S-5°N, 170°W-120°W. Used SSTa thresholds are defined as follows: (a) El Niño years include temperatures greater than 0.5°C above normal; (b) La Niña years include temperatures 0.5°C below normal; (c) neutral years are those that fall within these bounds. SSTa ONI data were obtained from the Climate Prediction Center (CPC) National Oceanic and Atmospheric Administration (NOAA) through http://www.cpc.ncep.noaa.gov/data/indices/. All three-year data used in this work were analyzed on a weekly basis because NOAA provides the SSTa data weekly. To make them directly comparable with SSTa ONI data, PWV data derived from GPS were sampled twice a day (00:00 UT and 12:00 UT) at the time of RS data availability. Then, both PWVs were converted to a daily average before further conversion to a weekly average.

3. RESULTS

3.1 COMPARISON OF PWV DETERMINED USING GPS AND RADIOSONDE DATA

The daily variation of PWV from GPS and Radiosonde measurements from 11 November to 20 December 2011 to detect ENSO is presented in Figure 2 for two of the areas (UMSK-WBKK and PIMO-TANAY) shown in Figure 1. The temporal interval has been selected according to the availability of both GPS and RS data. Results show a moderate correlation between GPS and RS measurements in both cases: for UMSK-WBKK we have R^2 = 0.59, while for PIMO-TANAY R^2 = 0.71, significant at the 99% confidence level. The moderate correlation may be due to topographical differences between the GPS and RS stations, in addition to random errors occurring in the data due to local weather or environment conditions. For 40 days observations, PWV data at UMSK (GPS) were 2.4 mm (in average) lower than PWV data at WBKK (RS). In contrast, in the other area, PWV data recorded at PIMO (GPS) were higher by approximately 1.0 mm (in average) than PWV data recorded at TANAY (RS) (~55 km from Manila). The root mean square error (RMSE) of PWV data between GPS and RS at the Malaysia station is 3.62 mm and 4.04 mm for data in the Philippines station.

As presented in Figure 2a, GPS data for ENSO studies could not be fully utilized because GPS data recorded at UMSK and RS data recorded at WBKK are missing for several days. Indeed, the daily average was chosen to minimize the gaps in the Radiosonde measurement stream, where the majority of data missing over the year was at 12:00 UT. Local extreme weather is one cause of data loss, which degrades the accuracy of daily mean. This resulted in a low correlation between GPS PWV and RS PWV. Typically, the accuracy of PWV obtained from GPS and RS measurements in normal weather conditions is around 7~10 mm as per results obtained by other researchers [e.g., Liu et al., 2000]. Heavy rainfall and high relative humidity, brought to the area around Borneo during the inter-monsoon period, can cause problems when launching RS balloons.

Additional causes for discrepancies between PWV values from GPS and RS data can be: (a) the distance between two systems is larger than 10 km (see Section 2.1); (b) topographical features, such as curvature, slope, and upslope areas that can influence the local hydrological conditions and soil moisture [e.g., Seibert et al., 2007]; (c) the difference in height above mean sea level between the GPS antennas and RS (see Table 1) that will also affect the correlation between GPS and RS measurements;
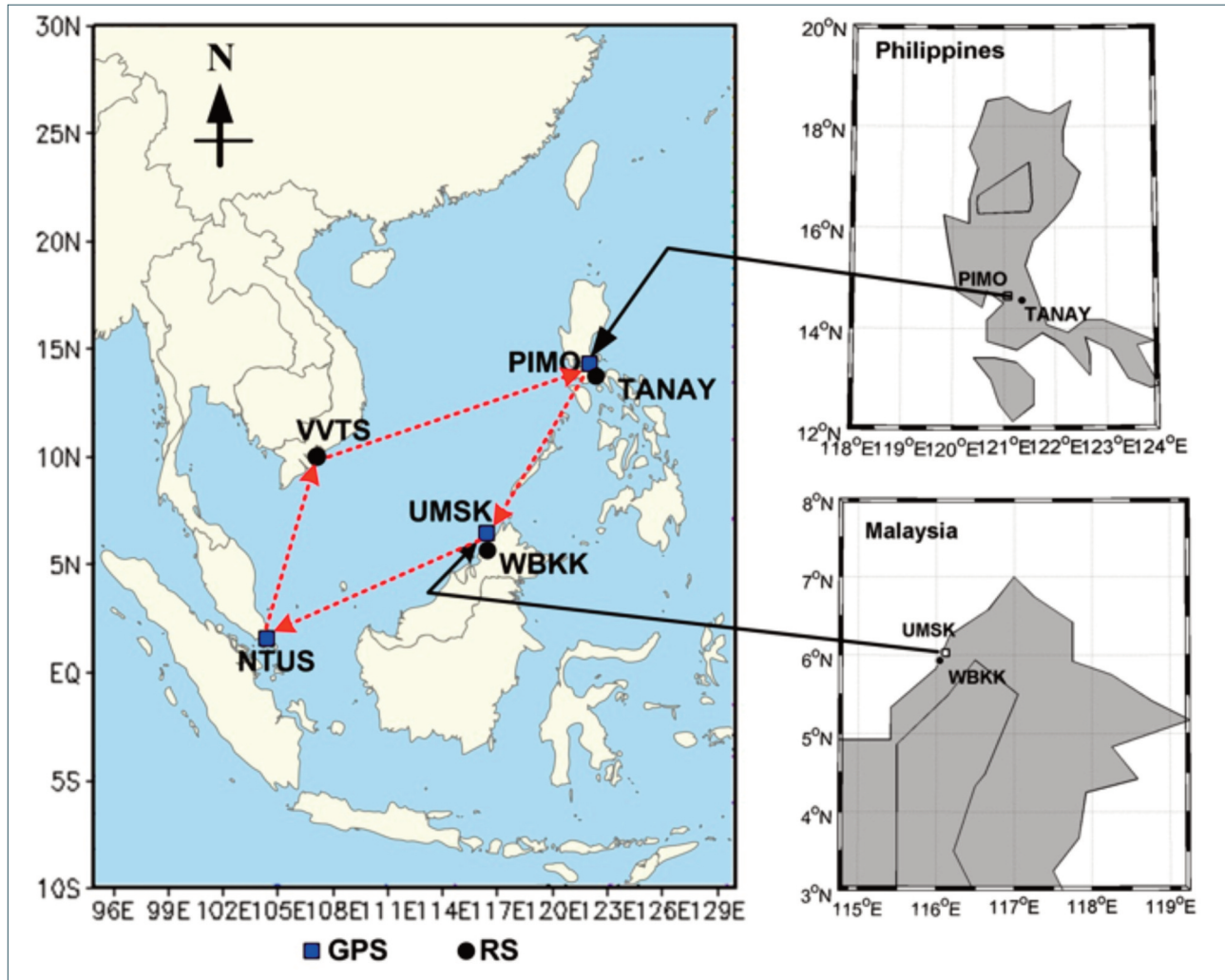
FIGURE 1. Location of the GPS stations (square) along with the RS stations (circle).

(d) the difference in accuracy and specifications of instruments used at each station. Nonetheless, overall the PWV values based on GPS and RS measurements exhibited an almost similar variation, with a good agreement to each other. This suggests that the availability of PWV data in the long-term can be useful for climate studies.

3.2 PWV VARIABILITY ALONG THE COAST OF SOUTH CHINA SEA

Figure 3 shows the daily variation of PWV from GPS and RS data from 1 January 2009 until 31 March 2011. Since there is no complete GPS data recorded at UMSK, PWV data from RS at WBKK was plotted as in Figure 3a with the aim of observing the annual variation. The argument for using this RS data is valid because the relationship between GPS PWV and RS PWV (see Figure 2) is well correlated with a positive trend. For the other locations, we use PWV from GPS at NTUS and PIMO (Figures 3b and 3d) and from RS at VVTS (Figure 3c). By comparing mean values, PIMO was 3.82 mm larger than UMSK; while for RS VVTS was 8.59 mm larger than NTUS. Note

also that no GPS data were recorded at NTUS for about 3 months between August and October 2009. For the four mentioned stations, selected in a clockwise direction (UMSK, NTUS, VVTS and PIMO) and falling within an area between 0°-6°N in latitude and 106-125°E in longitude, the range of PWV is between 26 mm and 56 mm (average value approximately 45.70 mm). To show the difference of PWV values between the stations, a delta (δ) is calculated based on Equation (9).

$$\delta_i = \left| X_i - \overline{X} \right| \tag{9}$$

where $\overline{X}$ is the mean of PWV from all the stations and X_i is the mean absolute value of PWV for each single station i. UMSK shows the highest δ value, which has been accidentally caused by unstable weather conditions and consequent loss of a significant amount of data. The average value of δ at four stations is obtained approximately 4.92 mm. Details of PWV and delta comparison at four selected stations are shown in Table 2.
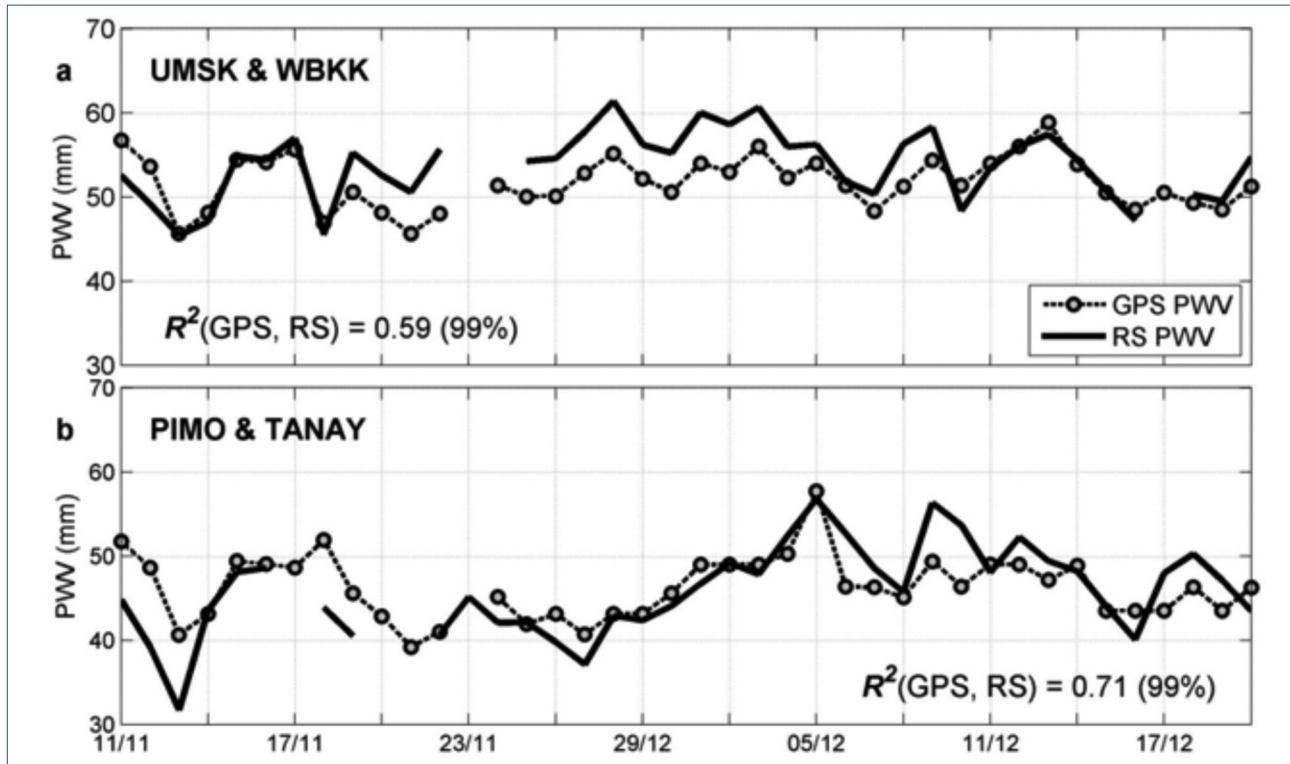
From Figure 3, there is no clear PWV pattern at UMSK

FIGURE 2. The comparison of PWV measurements on a daily average of both GPS and Radiosonde (RS) from November 11 to December 20, 2011 for (a) UMSK and WBKK (Borneo Malaysia) and (b) PIMO and TANAY (Philippines).
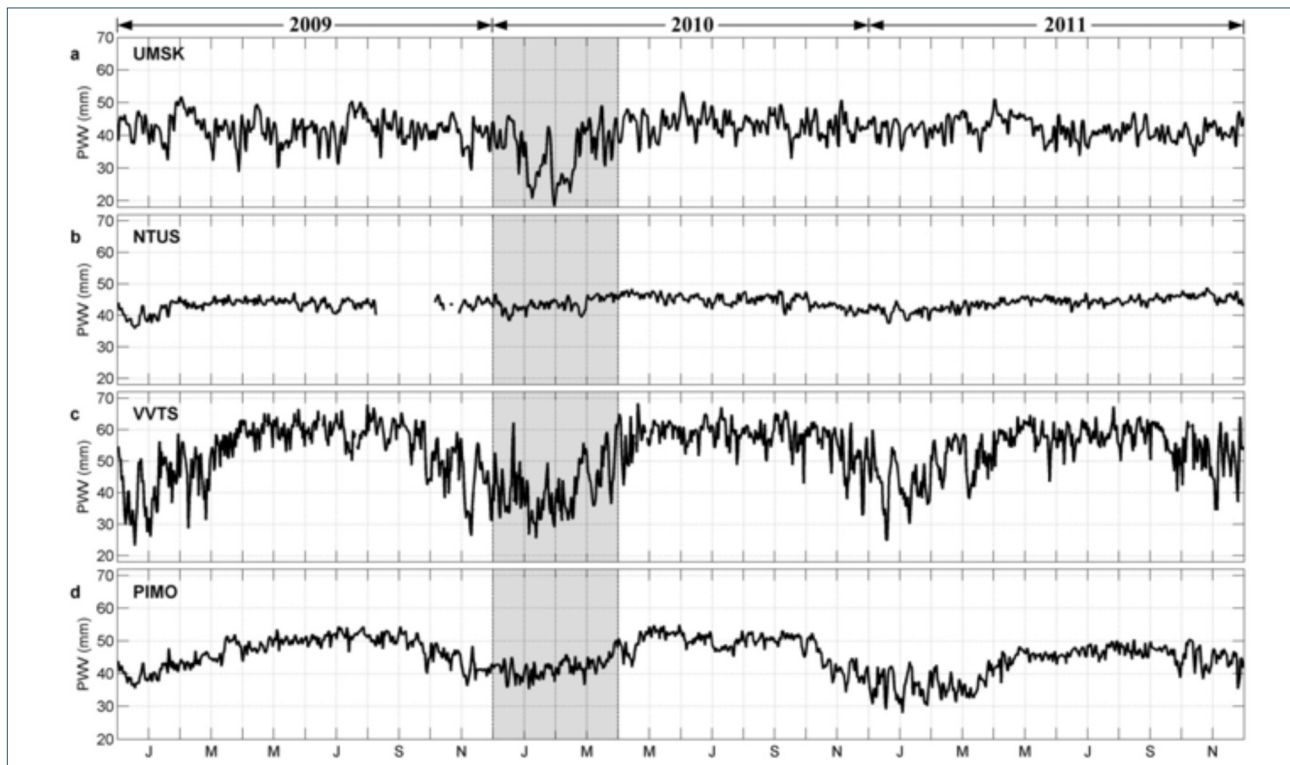

FIGURE 3. The daily average of PWV variation at two selected GPS stations (NTUS and PIMO) and at RS stations (UMSK and VVTS) along the coast of South China Sea for the period from January 1, 2009 to December 31, 2011. The shaded area shows a time span of El Niño event.

during the observation period as compared to PWV variations at VVTS and PIMO, except for drop during the El Niño event (see shaded area in Figure 3). Recorded PWV varies between 18 mm and 53 mm with an STD of 4.86

Station	MIN	MEAN	MAX	STD	Delta (δ)
UMSK	18.55	41.33	53.32	4.86	7.45
NTUS	35.86	43.86	48.78	2.11	4.92
VVTS*	23.21	52.46	68.35	9.22	3.68
PIMO	28.03	45.15	54.95	5.31	3.63
Average	26.41	45.70	56.35	5.37	4.92

TABLE 2. Comparison of the daily PWV measurements calculated based on the GPS and RS data for a 3-year period of observations. *RS station, $\delta_i = |X_i - \bar{X}|$. All PWV units are in mm.

mm. The variation of PWV at NTUS is moderately low but still follows the pattern of PWV at VVTS and PIMO. The difference value between the maximum and the minimum

of PWV for NTUS is 12.92 mm. The low variation of PWV at UMSK and NTUS stations is possibly due to the nearness of the stations to the equatorial line. Thus, the variation of PWV at VVTS and PIMO is more pronounced with a seasonal pattern, i.e. higher during the rainy season (middle of the year) and lower during the dry season (at the beginning and the end of the year). The rainy season usually begins in May and ends in late November, whereas the dry season lasts from December to April. In addition, the higher value of STD obtained in SCS regions (e.g., VVTS and PIMO) is possibly due to a strong interaction between the ocean and the air (ocean forcing). For both stations, the PWV data exhibit a moderate relationship with a correlation coefficient of 0.68 (significantly at the 99% confidence level). Despite this variation, a significant PWV drop to about 20 mm in February 2010 was observed at UMSK (see gray background). A similar drop was also observed at VVTS and PIMO, which indicates that it might be influenced by El Niño event at this time.
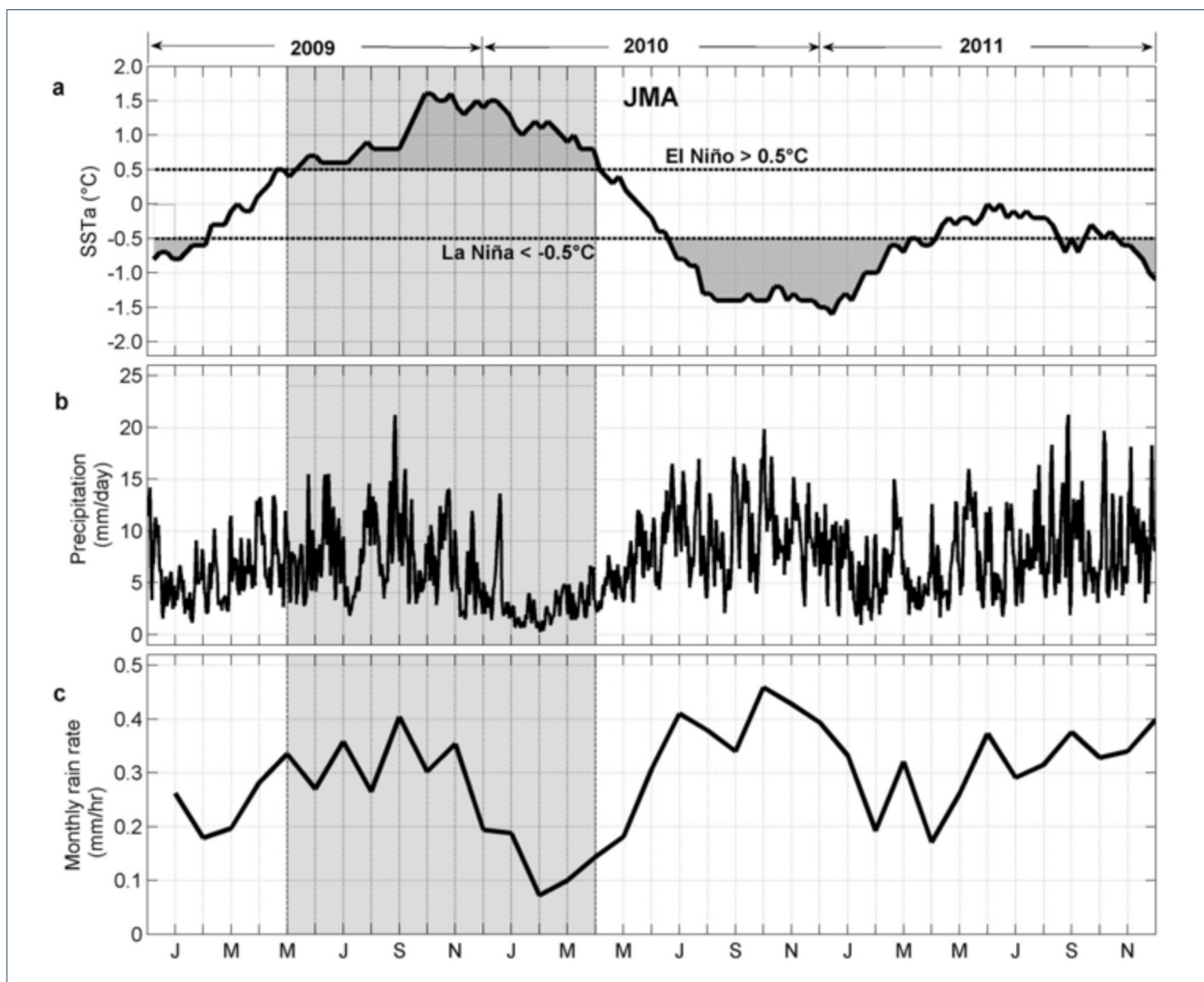
FIGURE 4. (a) Weekly variation of SSTa for the period of 2009 – 2011 from Niño 3.4 region, (b) daily precipitation recorded from TRMM (3B42.007), and (c) monthly rain rate recorded from TRMM (3B43.007). TRMM data are retrieved by TOVAS for the region: 100°E-125°E and 0°-16°N.

4. DISCUSSIONS

Figure 4 shows the association between ENSO and daily precipitation (mm/day) as well as monthly mean of rain rate (mm/hr) for the period from 1 January 2009 to 31 December 2011. In the first panel (Figure 4a), SSTa ONI data for Niño 3.4 region is used as an indicator of ENSO activity. According to the JMA definition, El Niño episode is identified to occur from May 2009 to April 2010 (see rectangle shaded area). Moreover, three La Niña episodes are also identified: from January to February 2009 (first episode), from July 2010 to April 2011 (second episode), and the last one from August to December 2011. The second episode is considered as a strong event with SSTa decreased to -1.8°C from the normal condition. The first and the last of La Niña events are regarded as a weak phase, and, therefore, will not be discussed further. Then the second and the third panels of Figure 4 (Figures 4b and 4c) shows the variation of precipitation and monthly rain rate based on the data taken by TRMM.

As shown in Figure 4, the La Niña event brings significant rainfall to the eastern side of the Malaysian Borneo. In this case, trade winds moved the event from Eastern Pacific to the Southern Pacific through part of the Southeast Asia region. As a result, severe weather, such as flooding, occurred in the Philippines and throughout the SCS region together with the region in Indonesia and Australia [Holden, 2013]. The variation of precipitation (Figure 4b) shows an almost similar trend to that of PWV in Figure 3, especially for VVTS and PIMO. For three years of observation, the daily precipitation is between 0.29 mm and 21.22 mm, with a maximum approximately in September and a minimum around February. A clear pattern of precipitation from monthly rain rate is presented in Figure 4c. Both precipitation and monthly mean of rain rate show an opposite pattern to the La Niña episode.

From Figures 4b and 4c, the daily precipitation and the monthly rain rate exhibited minimum values in February 2010, which are lower than those around February-April 2011. This minimum peak is possibly due to the residual effect of El Niño event after its peak in December 2009. To clarify the climate response to ENSO event during 2009/2010 at all selected stations, SSTa above 0.5°C (El Niño episode) is analyzed (see gray background in Figure 3 and 4). The PWV and precipitation data on a daily basis at each station are averaged weekly following the GPS calendar (from 4 January 2009 to 31 December 2011). The weekly PWV is then correlated with SSTa. The weekly average of both parameters is then filtered by applying a moving average with a window of 5 weeks to smooth short-term fluctuations and highlight longer-term variability.

The analysis of PWV and precipitation during both El Niño and La Niña periods is presented in Figure 5. Figure 5a (left side) shows that the El Niño peak occurred at GPS week 1553 with SSTa reaching 1.9°C. In Figure 5b (left side), PWV exhibited almost similar variation at all stations with maximum and minimum values appearing at GPS week 1540 and 1563, respectively. A variation in precipitation comparable to the trend of PWV is also shown in Figure 5c (left side). Note that in Figure 5c, the solid lines show the precipitation data from TRMM for the region: 100°E-125°E and 0°-16°N whereas dashed lines show the precipitation average at the four considered locations. The relationship between PWV and precipitation for this El Niño period demonstrated a very strong correlation (R^2 = 0.80 significantly at the 99% confidence level). Comparing PWV and SSTa in Figure 5 (left side), it is apparent that the occurrence of El Niño affects the region of SCS approximately 10 weeks later. This impact is indicated by a minimum peak of PWV which is more pronounced at UMSK and less at NTUS. Table 3 summarizes the comparison of PWV amount during the 2009/2010 El Niño events as compared to the normal condition.

The 10 weeks delays of PWV and rainfall with respect to the El Niño episode is due to the weakening of easterly trade winds over the equatorial Pacific Ocean and blew of warmer surface water westward (SSTa increased), which brought convective storms to the Philippines, Indonesia, and the coastal of Australia. The first indication is the decrease of PWV average at all stations by about 14% as compared to the normal condition (see Table 2). The decreasing in sea surface temperature due to changes in the circulation of air mass over time reduces the formation of rain clouds in the atmosphere. The ocean temperatures warmer than usual will result in low rains (atmosphere is drier) and can cause drought in the western Pacific. On the other hand, along with the increasing intensity of El Niño, the high rainfall is shifted towards the South as described by Holden [2013]. The origin of all these phenomena is usually coming from interactions between the oceans and the atmosphere. The propagation of Pacific trade winds from east to west will decrease the moisture content in the atmosphere due to warm water moved eastward. The air atmosphere will be drier (low moisture content) since the sunlight stored their energy in the ocean and sea surface temperatures become warmer. As a result, atmospheric water vapor (PWV) presents an inverse correlation with SSTa.

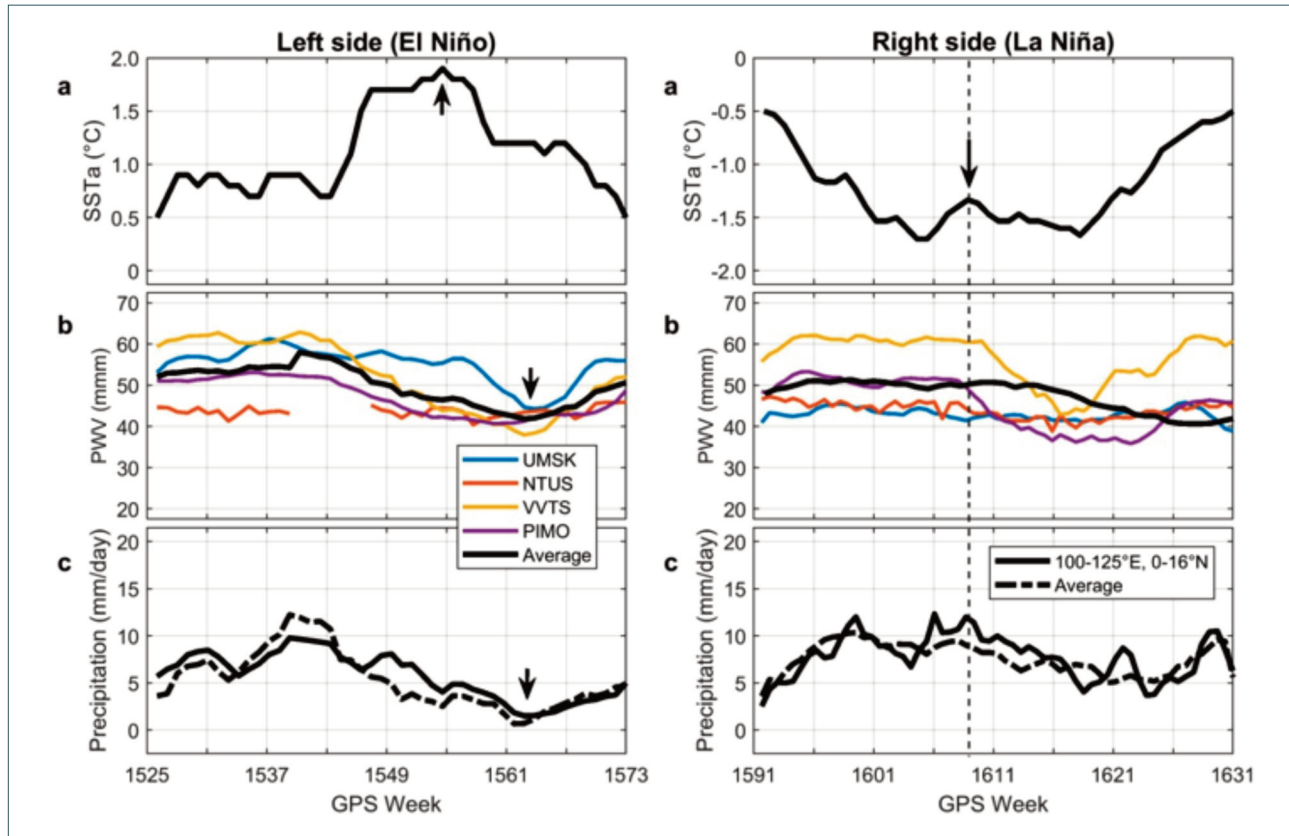For La Niña case of Figure 5 (right side), which is

FIGURE 5. Association between PWV and precipitation on SSTa during 2009/2010 El Niño (left side) and 2010/2011 La Niña (right side) periods. The solid lines in Figure 5c shows TRMM data for the area 100°E-125°E and 0°-16°N and the dashed lines shows the average value at four stations.

Station	El Niño		La Niña		Remark
	δ PWV (mm)	δ Precipitation (mm/day)	δ PWV (mm)	δ Precipitation (mm/day)	
UMSK	3.01	1.88	0.39	2.27	The average values during normal conditions are 48.11 mm and 7.21 mm/day for PWV and precipitation, respectively.
NTUS	1.22	1.22	2.22	1.31	
VVTS	5.66	0.91	3.21	2.35	
PIMO	0.95	3.13	2.94	2.37	
Average	2.71	1.78	2.19	2.07	

TABLE 3. The comparison of PWV and precipitation averages at four selected stations during the period of 2009/2010 El Niño and 2010/2011 La Niña.

characterized by a low value of SSTa (-1.8°C), the activity leads to significant changes to PWV and precipitation, as shown in right side of Figures 5b and 5c, respectively. During an increasing phase of La Niña (down arrow on the right column of Figure 5), both PWV and precipitation are increased. Figure 5b (right side) highlights that PWV decreases when the intensity of La Niña start to decrease and, afterwards, continues to decrease following the trend of SSTa. This confirms that there is a positive correlation of both PWV and precipitation with SSTa during La Niña event. This feature is more pronounced at the VVTS and PIMO stations

than at the UMSK and NTUS stations. A detailed comparison of PWV changes during the 2010/2011 La Niña event is summarized in Table 3. Note that the normal condition in table is computed based on the -0.5°C ≤ SSTa ≤ 0.5°C, where δ is the variability of the respective parameter with respect to its normal conditions. The δ is obtained by $\delta_i = |X_i - \bar{X}|$, where $\bar{X}$ and X_i are the average value over 3 years and the absolute value of PWV or precipitation for each station, respectively. During El Niño, UMSK and VVTS show the highest δPWV, while PIMO shows the highest precipitation. Moreover, during La Niña, PIMO and VVTS

experienced an increase in both PWV and precipitation. On the other hand, VVTS and PIMO are in line with NASA release (http://trmm.gsfc.nasa.gov/publications_dir/philippine_flooding_20dec10-19jan11.html) which states that heavier rainfall has occurred, particularly for the period from 20 December 2009 to 11 January 2010, when the average of precipitation has reached more than 100 mm per day. As a result of this event, the precipitation of approximately 6,000-7,000 mm in 2011 brought floods and landslides over the Philippines. The above results show that all stations are affected by El Nino and La Nina with different intensity.

On the occurrence of La Niña, the basic mechanism of how the GPS water vapor responds to this event can be explained as follows. Referring to Figure 5 (right side), PWV was found to be high when the SSTa is a maximum. This shows that the strengthening of easterly trade winds around the equator, as the result of an increase in the pressure difference between the eastern and western tropical Pacific, affects the sea surface temperature. A stronger easterly trade wind flow pushes the colder water from the bottom of the ocean surface to the western Pacific and then brings increased precipitation over the western and central tropical Pacific. In other words, during the La Niña event, heavy rainfalls tend to occur in the equatorial Pacific Ocean because the sea surface temperature is colder than usual in the tropics. It is clear that the heat of the ocean current moving to the western Pacific leads to a reduction in air pressure along the pathways Niño region. Reduced air pressure increases the air expansion and cooling, so the water condenses out of the atmosphere and forms a cloudy or rainy weather. This suggests that during heavy rains, the upwelling and cooling of the sea surface increases; as a result, water vapor content in the atmosphere is reduced. Note that, depending on many factors, the occurrence of heavy rain is not always accompanied by a decrease in the content of atmospheric water vapor as detected by the GPS and RS.

5. CONCLUSIONS

This paper reported the application of GPS and radiosonde meteorology for climate studies such as investigating the correlation of the water vapor variability with ENSO events. The use of GPS PWV measurements to detect and characterize a specific climate event, such as ENSO, is innovative, particularly with respect to the targeted region.

The findings can be summarized as follows. From the comparison of PWV observation at two selected GPS and RS stations in the Niño 3.4 region, GPS PWV at PIMO shows a good agreement with RS PWV along 40-day period. For a three-year observation (2009-2011) at four selected locations in SCS, changes in PWV were significantly influenced by seasonal variations. For VVTS and PIMO, seasonal patterns appear to be maximum in dry (hot) season and minimum in rainy (wet) season, while the PWV peak for UMSK and NTUS increases during the intermonsoon periods. The response of climate variation during the El Niño phase SSTa increases in Niño regions, consisted in the decrease of PWV which dropped about ten week later, after SSTa has peaked. This climate response has been explained with the variation of precipitation measured by TRMM. The occurrence of El Niño brought unusually dry conditions (lower rainfall) affecting the western Pacific Ocean and SCS, and this condition influences the meteorological pattern by decreasing the value of GPS PWV data. In contrast, the impact on climate during 2010/2011 La Niña event consisted in an increase of the PWV value and rainfall amounts.

In conclusion, the occurrence of ENSO activity disrupts the normal circulation pattern over the Pacific oceans and affect the climate parameter in a way that can be detected indirectly by GPS receiver measuring PWV. Looking at the study area and the period of investigation, PWV has demonstrated an inverse relationship with El Niño index. El Niño is associated with weaker of trade winds. To improve forecast models, the mechanism by which GPS PWV contribute to the phases of ENSO will be studied in future work by collecting long-term GPS data and ancillary data.

REFERENCES

Bajželj, B., and K. S. Richards (2014). The positive feedback loop between the impacts of climate change and agricultural expansion and relocation. Land, 3, 898-916.

Bevis, M., S. Businger, T. A. Herring, R. A. Anthes, C. Rocken, and R. H. Ware (1992). GPS meteorology: Remote sensing of atmospheric water vapor using the Global Positioning System. J. Geophys. Res., 97, 15787-15801.

Bevis, M., S. Businger, and S. Chiswell (1994). GPS meteorology: Mapping zenith wet delays onto precipitable water. J. Appl. Meteorol. 33 (3), 379-386.

Chen, G., and H. Lin (2005). Impact of El Niño/La Niña on the seasonality of oceanic water vapor: a proposed scheme for determining the ITCZ. Mon. Wea. Rev., 133, 2940–2946.

J. Davis, T. Herring, I. Shapiro, A. Rogers, and G. Elgered, "Geodesy by radio interferometry: Effects of atmospheric modeling errors on estimates of baseline length," Radio Sci., 20, 1593-1607, 1985.

Hofmann-Wellenhof, B., H. Lichtenegger, and J. Collins (2001). *Global Positioning System: Theory and Practice.* 7th rev. edn., Springer.

Holden, W. N. (2013). Neoliberal mining amid El Niño induced drought in the Philippines. J. Geograp. Geolog., 5, 58-77.

Japan Meteorological Agency (JMA) (1991). Marine Department: Climate charts of sea surface temperatures of the western north pacific and the global ocean.

Liu, Y., C. Yonggi, and L. Jingnan (2000). Remote sensing of atmospheric water vapor using ground-based GPS data. Geo-spat. Inform. Sci., 3, 64-68.

Klein Baltink, H., H. J. P. Derks, A. C. A. P. Van Lammeren, B. A. C. Ambrosius, A. G. A. Van Der Hoeven, H. Van Der Marel, F. Kleijer, and A. J. M. Kosters (1999). Water vapour from GPS tropospheric delay estimates, In: GPS water vapour meteorology, Beleids Commissie Remote Sensing (BCRS), Chapter 2, pp 3-11.

Pokhrel, S., H. S. Chaudhari, S. K. Saha, A. Dhakate, R. K. Yadav, K. Salunke, S. Mahapatra, and S. A. Rao (2012). ENSO, IOD and Indian Summer Monsoon in NCEP climate forecast system. Clim. Dyn., 39, 2143–2165.

Qian, J. H., A. W. Roberston, and V. Moron (2013). Diurnal cycle in different weather regimes and rainfall variability over Borneo associated with ENSO. J. Clim., 26, 1772-1790.

Saastamoinen, J (1972). Introduction to Practical Computation of Astronomical Refraction, Bull. Geodesique, 106, 383-397.

Seibert, J., J. Stendahl, and R. Sørensen (2007). Topographical influences on soil properties in boreal forests. Geoderma, 141, 139 – 148.

Suparta, W., Z. A. Abdul Rashid, M. A. Mohd Ali, B. Yatim, and G. J. Fraser (2008). Observation of Antarctic precipitable water vapor and its response to the solar activity based on GPS sensing. J. Atmos. Sol-Terr. Phys., 70, 1419-1447.

Suparta, W., M. S. Jit Singh, M. A. Mohd Ali, B. Yatim, and A. N. Mohd Yatim (2011). GPS water vapor monitoring and TroWav updated for ENSO studies. Proceeding of the 2011 International Conference on Instrumentation, Communication, Information Technology and Biomedical Engineering (ICICI-BME 2011), Bandung, Indonesia, 8-9 November 2011, pp 35-39.

Suparta, W., A. Iskandar, M. S. Jit Singh, M. A. Mohd Ali, B. Yatim, and A. N. Mohd Yatim (2013). Analysis of GPS water vapor variability during the 2011 La Niña event over the western Pacific Ocean. Ann. Geophys., 563, R0330, doi:10.4401/ag-6261.

Suparta, W. and A. Iskandar (2013). Modeling of Weighted Mean Temperature Over the Western Pacific Region to Estimate GPS PWV. Proceeding of the 2013 IEEE International Conference on Space Science and Communication (IconSpace2013), Melaka, Malaysia, pp. 190-193, doi: 10.1109/IconSpace.2013.6599462.

Suparta, W. (2014). The development of GPS TroWav tool for atmospheric – terrestrial studies. J. Phys. Conf. Ser., 495, 012037, doi:10.1088/1742-6596/495/1/012037.

Trenberth, K. E. (1997). The Definition of El Niño. Bull. Amer. Met. Soc., 78, 2771-2777.

*CORRESPONDING AUTHOR: Wayan SUPARTA,
Department of Doctor of Computer Science,
Bina Nusantara University,
Jakarta, Indonesia

email: drwaynesparta@gmail.com